High-Resolution X-ray Diffraction of Muscle Using Undulator Radiation from the Tristan Main Ring at KEK†

Katsuzo Wakabayashi,[a]* Hiroshi Sugiyama,[b] Naoto Yagi,[c] Thomas C. Irving,[d] Hiroyuki Iwamoto,[e] Keisuke Horiuti,[f] Yasunori Takezawa,[a] Yasunobu Sugimoto,[a] Masaki Ogino,[a] Shigetoki Iino,[a] Duck-Sool Kim,[a] Toshikazu Majima,[g] Yoshiyuki Amemiya,[h] Shigeru Yamamoto[b] and Masami Ando[b]

[a]*Division of Biophysical Engineering, Graduate School of Engineering Science, Osaka University, Toyonaka, Osaka 560, Japan,* [b]*Photon Factory, Institute of Materials Structure Science, High Energy Accelerator Research Organization (KEK), Tsukuba, Ibaraki 305, Japan,* [c]*SPring-8, Japan Synchrotron Radiation Research Institute (JASRI), Kamigori, Hyogo 678-12, Japan,* [d]*BioCAT, Department of Biological, Chemical and Physical Sciences, Illinois Institute of Technology, Chicago, Illinois 60616-3793, USA,* [e]*Department of Physiology, School of Medicine, Teikyo University, Itabashi-ku, Tokyo 173, Japan,* [f]*Department of Physiology, Oita Medical University, Hasama, Oita 879-55, Japan,* [g]*Supermolecular Science Section, Electrotechnical Laboratory, Tsukuba, Ibaraki 305, Japan, and* [h]*Engineering Research Institute, Faculty of Engineering, The University of Tokyo, Bunkyo-ku, Tokyo 113, Japan. E-mail: waka@bpe.es.osaka-u.ac.jp*

High-resolution X-ray diffraction studies on striated muscle fibres were performed using a hard X-ray undulator installed in the Tristan main ring at KEK, Tsukuba, Japan. The performance of the undulator, along with an example experiment which exploited the unique characteristics of undulator radiation, are reported. The vertical divergence angle of the first harmonic of the undulator was $\sim$10 µrad under 8 GeV multi-bunch operating conditions and the peak photon flux density was estimated to be $\sim$3 $\times$ 10^{16} photons s^{-1} mrad^{-2} (0.1% bandwidth)$^{-1}$ (10 mA)$^{-1}$. The well collimated X-ray beam from the undulator made it possible to resolve clearly, with high angular resolution ($\sim$700 nm), the closely spaced diffraction peaks on the meridional axis in the X-ray patterns arising from the thick filaments of a striated muscle under static conditions. By fitting the meridional intensity pattern, a model for the molecular arrangement of the constituent proteins in the thick filaments is proposed. These studies of muscle demonstrate the promise of undulator radiation from third-generation sources for high-resolution diffraction studies.

1. Introduction

X-ray fibre diffraction has for many years played a key role in studying the molecular mechanism of muscle contraction. This arises from its ability to investigate muscle structures under native physiological conditions and also because it can, at least in principle, detect global changes in sarcomere structure at the physiologically relevant timescale. These kinds of experiments make unusually high demands on X-ray sources and optics (see Huxley & Brown, 1967; Holmes, 1989). Muscle diffracts relatively weakly, has many components with similar long spacings, and the changes of physiological states in muscle and the accompanying structural changes occur in a timescale of milliseconds or a few hundreds of micro-seconds. Lack of X-ray flux necessary to resolve these motions motivated the very first biological experiments using synchrotron radiation (Rosenbaum *et al.*, 1971; Holmes, 1974), which in turn helped provide the impetus for the construction of second-generation dedicated synchrotron sources with specialized small-angle X-ray beamlines. Recent years have seen the construction of high-energy third-generation sources such as the ESRF, the APS and now the SPring-8, which have been optimized for insertion devices such as hard X-ray undulators. The Tristan Super Light Facility at KEK would have been an additional such third-generation light source with some innovative characteristics, and was designed to direct a fourth-generation light source (see Tristan Super Light Facility Conceptual Design Report, 1992; Kamada *et al.*,

† High Energy Accelerator Research Organization (KEK), Tsukuba, Japan.

1995; Yamamoto *et al.*, 1995). The Tristan main ring synchrotron has a circumference of 3018 m, the largest among those used as a storage ring, ensuring low emittance. The main ring, however, was available for synchrotron radiation experiments for only a six-month period in the latter half of 1995 (due to the reconstruction for the B-factory project), about half of which was spent installing an undulator, a beamline and reconstructing an accelerator for the experiments using synchrotron radiation. Undulators, in addition to the higher flux expected over bending-magnet sources, can be envisaged to yield higher-quality X-ray diffraction patterns from biological and other substances because of their very low source divergence. Using the main ring beamline (Sugiyama, 1996; Sugiyama *et al.*, 1998) we were able to acquire static X-ray diffraction patterns with exceptionally high spatial resolution which have been used to deduce a model for the distribution of myosin crossbridges projecting along a thick filament in a striated muscle. In addition to the experiment described here, we have previously reported experiments performed using this apparatus which probed crossbridge states in the striated muscle by collecting one-dimensional time-resolved diffraction data using a rotating-drum image-plate system from chemically demembraned muscle fibres when sinusoidal length perturbation was applied during active contraction and in rigor (Yagi *et al.*, 1996).

2. Results and discussion

2.1. Performance and characterization of the undulator beamline at the Tristan main ring

The Tristan main ring was commissioned to operate at a beam energy of 8 or 10 GeV with a maximum beam current of 16 mA. A 5.4 m undulator was constructed using a modular design, with length 1.8 m and a period of 4.5 cm × 40 periods with a maximum K value of 1.11 (for details, see Yamamoto *et al.*, 1997). The vertical/horizontal divergence angle of an 8.5 keV beam at the first harmonic from this device was calculated to be 15/95 µrad, so that the expected beam size would be ~1.5 mm (V) × 9.7 mm

(H) at 100 m from the source with a total flux of ~1 × 10^{14} photons s^{-1} at 10 mA. The optical arrangement used for the present experiments is shown in Fig. 1 (see also Fig. 1 in Yagi *et al.*, 1996). The first cryogenically cooled Si 220 monochromator was located at about 87 m from the source. A second Si 220 monochromator of the double-crystal monochromator (Sugiyama, 1996; Sugiyama *et al.*, 1998) was set 4.5 m down (Fig. 1), where the experimental room was located, at about 100 m from the source point. The vacuum duct component of welded bellows allowed the second crystal to move horizontally for about 2.7 m to permit a wide range of selected beam energies. Scattering angles available were in the range 36–52°, corresponding to available beam energies of 10.5–7.4 keV at Si 220 diffraction. There was no evidence for thermal degradation of beam intensity, showing that cooling of the first monochromator was adequate.

The vertical divergence angle of the first harmonic of undulator radiation was measured on a number of occasions during operation of the main ring. We used $(-, +, +)$ Si 220 or 400 settings corresponding to the first, second and analyser crystals, respectively, for the measurements (Sugiyama, 1996; Sugiyama *et al.*, 1998). Fig. 2 shows the vertical angle dispersion, $\sigma_{y'}$, as a function of ring current. $\sigma_{y'}$ dramatically increased at currents over 1 mA in single-bunch operation. In multi-bunch operation, however, the increase of $\sigma_{y'}$ was small even at several milliamps of total ring current since each bunch was now under 1 mA current. $\sigma_{y'}$ was also examined as a function of undulator gap. The results showed that $\sigma_{y'}$ was proportional to the magnetic flux density which related to the undulator gap or K value. Since $\sigma_{y'}$ was observed to increase with increased magnetic flux density, there were extra horizontal magnetic field components in the undulator. We were able to apply corrective horizontal magnetic fields to eliminate this increase in $\sigma_{y'}$. $\sigma_{y'}$ was about 10 µrad in the experiment reported here where the main ring was operated at 8 GeV
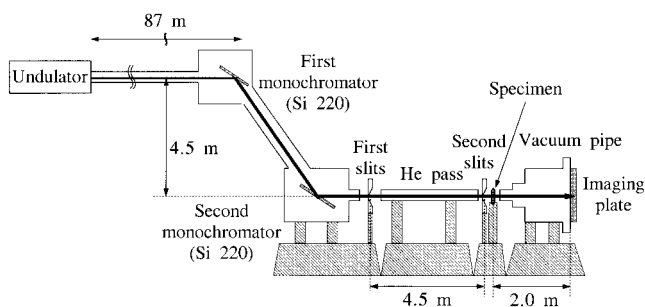
Figure 1
The optical arrangement used for high spatial resolution diffraction experiments on muscles. The Si monochromator crystals were adjusted to pass the first harmonic of the undulator beam (8.5 keV). The first monochromator was cryogenically cooled by liquid nitrogen.
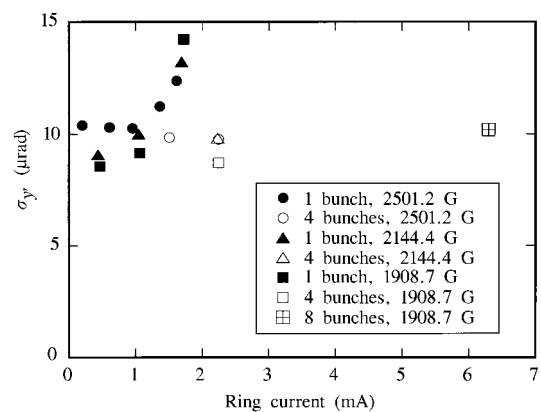
Figure 2
The vertical angle divergence, $\sigma_{y'}$, of the electron beam measured as a function of ring current. Closed symbols show $\sigma_{y'}$ in single-bunch operation and open ones show $\sigma_{y'}$ in multi-bunch (four or eight bunches) operation. Other numerical values denote the magnetic flux density of the undulator (which relates to the undulator gap) in the measurements.

in multi-bunch with each bunch under 1 mA current and the undulator had a K value of 1.08 without any corrective magnetic fields.

Fig. 3 shows the measured photon flux density with 10 mA beam current, a beam energy of 10 GeV, $K = 1.09$ of the undulator and with corrective magnetic fields applied during the measurements (Sugiyama, 1996; Sugiyama *et al.*, 1998).

Each measured flux density is shown as closed circles and the theoretical values (Yamamoto *et al.*, 1997, 1998) as a solid curve. Since we did not measure a spectrum with 8 GeV beam energy, a spectrum at 8 GeV was calculated under conditions of the muscle experiments using parameters determined from the 10 GeV spectrum. From the calculation, the peak photon flux density at the first harmonic was estimated to be $\sim 3 \times 10^{16}$ photons s^{-1} $mrad^{-2}$ (0.1% bandwidth)$^{-1}$ (10 mA)$^{-1}$.

2.2. High-resolution X-ray small-angle diffraction on resting striated muscle

The ring energy was set to 8 GeV with beam currents of about 1–8 mA. The magnetic flux density in the undulator was 2570 G. The K value of the undulator was 1.08 without corrective magnetic fields. The Si 220 monochromators were adjusted to pass the first harmonic of the undulator beam at 8.5 keV. In the static experiments reported here, no focusing optics were used (Fig. 1). Two pairs of remotely adjustable vertical and horizontal slits, one just behind the second monochromator, the other just before the sample 4.5 m downstream, were used to collimate the beam. The first pair of slits limited the beam size to 0.14 mm (V) × 0.57 mm (H). The second pair were used as guard slits which cut the parasitic scatter from the edges of the first slits. The beam size after the second slits was 0.16 mm × 0.60 mm at the specimen position. A 20 μm
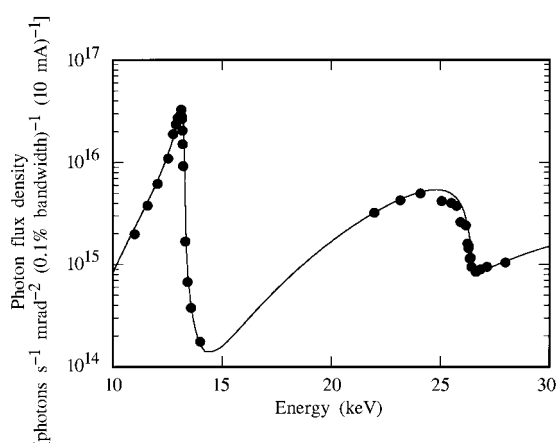

Figure 3
A spectrum of the undulator radiation at 10 GeV operation of the main ring. The data were taken from Sugiyama *et al.* (1998). Closed circles show measured values and the solid curve shows the theoretical calculation (see Yamamoto *et al.*, 1997, 1998).

increment in the vertical beam size over a 4.5 m travelling distance indicates a very small divergence of the undulator beam. The flux under these conditions was $\sim 5 \times 10^8$ photons s^{-1} at a ring current of 5 mA. The two monochromator crystals were slightly detuned in order to suppress the second harmonic of the undulator spectrum. X-ray diffraction patterns were recorded on an image plate (Fuji Film, type BAS-III) which was scanned with a 100 μm pixel size using a BAS 2000 scanner (Fuji Film, Tokyo, Japan).

Fig. 4(a) shows an X-ray diffraction pattern taken from a frog (*Rana catesbeiana*) live sartorius whole muscle resting in a Ringer solution with its longitudinal axis oriented vertically. The exposure time was 30 min on an image plate with a ring current of about 4 mA, and the specimen was continuously moved slowly up and down during the exposure to avoid radiation damage. Because of the small vertical divergence of the beam, and the low background from this instrument, we were able to obtain X-ray patterns of exceptionally high quality showing over 100 fine-intensity peaks along the meridian (the central vertical axis) in the reciprocal Bragg spacing region of 0.015–0.25 nm^{-1}. Fig. 4(b) shows an intensity tracing on the meridian after multiplication by the square of the axial coordinate and subtraction of background intensity. These fine peaks, with a peak-to-peak separation of 700–1000 nm, arise from interference effects of the long-range periodicities within the muscle. We can interpret these fine peaks in the pattern with reference to what we know of the detailed substructure of muscle. Striated muscle is composed of many thousands of repeating units called sarcomeres which are linked on either end by structures called Z lines. The sarcomeres in our muscle specimen are about 2.3 μm long. Because sarcomeres are not so homogeneous in length, any sampling effect due to these long repeats disappears in the spacing region resolved in the present pattern (see Bordas *et al.*, 1987). In electron micrographs of the longitudinal section of muscle, many long-range periodic structures can be seen (see Squire, 1981; Craig *et al.*, 1992). These may originate from the mass projection along the sarcomere axis of density from a number of protein molecules known to be located in the myofilaments within sarcomeres. These include myosin, C-protein and possibly titin/connectin molecules in the thick filament and the assembly of the thin filaments containing actin, tropomyosin, troponin and possibly nebulin molecules. We can explain the intensity distribution due to the thick-filament-based reflections on the basis of just two of these proteins, the arrangements of so-called myosin crossbridges (consisting of two globular heads and an α-helical coiled-coil tail) around the thick filament and of C-protein molecules which occur at distinct locations along the thick filament (Squire, 1981). Both myosin crossbridges and individual C-protein molecules on the thick filaments are arranged symmetrically in each half of the sarcomere so that they diffract coherently leading to many fine peaks in the meridional pattern. The intensity tracing in Fig. 4(b)
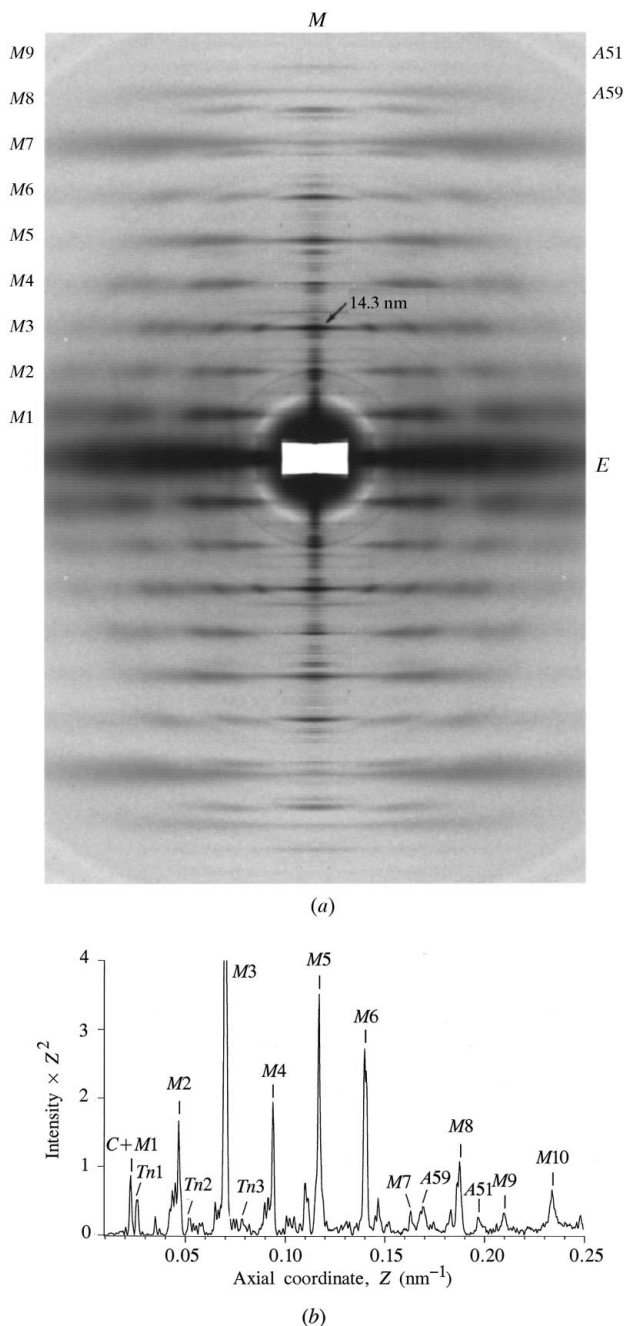
(a)

(b)

Figure 4

(a) An example of X-ray diffraction patterns taken from frog skeletal muscles in the living relaxed state. The pattern was recorded on an image plate with an exposure of 30 min at a camera length of 2 m and a ring current of ~4 mA. The background intensity was appropriately subtracted for illustration purposes. The fibre axis of the muscle is vertical. *M*: meridional axis. *E*: equator. *M*1–*M*9: thick-filament-based layer lines indexed on the 42.9 nm repeat. *A*51, *A*59: 5.1 and 5.9 nm thin-filament-based layer lines. (b) Intensity profiles on the meridian in the X-ray pattern in (a). Intensities shown have been multiplied by the square of the axial coordinate. *M*2–*M*10: thick-filament-based meridional reflections with a basic repeat of 42.9 nm. *C*: a 44 nm reflection, possibly from C-protein arrangements on the thick filaments. *Tn*1–*Tn*3: reflections with a repeat of 38 nm from troponin molecules on the thin filaments. All fine peaks come from the sampling by the long-range periodicities in a sarcomere (see text). Contamination from the second harmonic was ~5%.
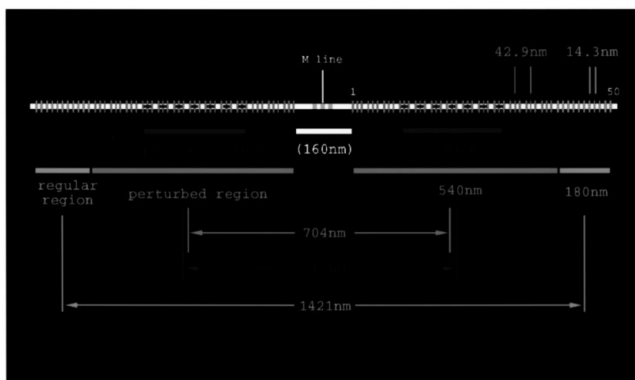
shows that the peak-to-peak separation of the fine peaks sampling the thick-filament-based reflections (labelled *M*) was about 704 nm (corresponding to an angular resolution of $\sim 2 \times 10^{-4}$ rad) and that of the peaks sampling the thin-filament-based reflections (labelled *Tn* in Fig. 4b) was about 1000 nm. Thus, the main ring undulator has enabled the recording of very high spatial resolution patterns in the axial direction.

2.3. *Analysis of the meridional intensity distribution due to the thick filaments*
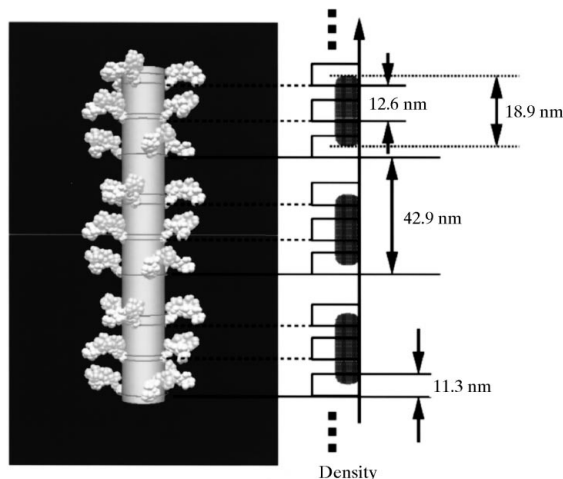
X-ray diffraction patterns from relaxed frog muscle show a series of layer lines indexing on an axial repeat of 42.9 nm, which are denoted by *M* in Fig. 4(a). The dominant features of the pattern are attributed to the helical structure of the three-stranded thick filament. Analysis of the high-resolution meridional intensity data has allowed us to propose a one-dimensional model for the thick filament in frog sartorius muscle. Thick filaments are 1.6 µm long with myosin crossbridges located at about 50 projection levels in each half of the filament with an average period of 14.3 nm (see later, Fig. 5a). The interaction of these crossbridges with actin in the thin filaments is responsible for muscle contraction. In the region of the thick filament containing the projections it has been suggested that an axial perturbation of the crossbridge levels occurs with a period of about 43 nm (= 14.3 nm × 3) forming a triplet structure of projections (Yagi *et al.*, 1981; Stewart & Kensler, 1986; see Fig. 5a). The average sampling period on the reflections, except on three multiple orders of the 42.9 nm repeat, was 704 ± 5 nm, corresponding to the centre-to-centre distance of the two perturbed regions. Thus, the perturbed region covers the central region of the thick filaments while distal parts of the filaments have projection levels that are regularly ordered on the 14.3 nm repeat. The unperturbed distal ends of the filament are then separated by ~1421 nm. The three multiple-order reflections may be sampled by this separation length. On the thick filaments there are, in addition, C-protein and titin/connectin molecules bound. Since the binding mode of the titin/connectin molecules is still unclear, we consider here only C-protein molecules as accessary proteins. The periodicity of the C-protein molecules bound to the filaments seems to be close to 43 nm (Huxley & Brown, 1967) or slightly larger than this (Rome *et al.*, 1973; Haselgrove, 1975). The interference period of ~710 nm on the first meridional reflection in the pattern may come from the distance between these two C-protein-containing regions (see also, Haselgrove, 1975). Note that the C-protein binding region covers only part of the crossbridge perturbed region. Fig. 5(a) represents a protein arrangement incorporating these features, with the help of electron microscopic evidence.

In modelling studies, we assumed a mixed structure of a thick filament consisting of the perturbed and unperturbed regions of crossbridge projecting levels incorporating C-protein molecules in the former region (Fig. 5a). In the

perturbed region, the thick filament has a triplet structure with three successive crossbridge levels and the perturbation was described by the separation between levels in the triplet. The axially projected density profiles of individual crossbridge projecting and C-protein binding levels were approximated by box functions which were defined by their axial lengths and total weights, respectively. The best fit to the observed data was found by varying several of the parameters mentioned above. Fig. 5(b) shows part of a proposed structure of the crossbridge perturbed region
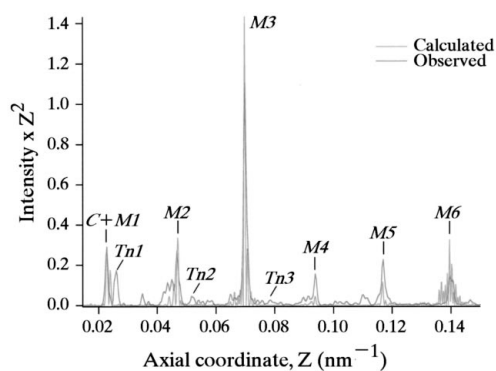

Figure 6
Comparison of the calculated meridional intensities from the best-fit one-dimensional model in Fig. 5 and the observed ones. C: the C-protein reflection (including the $M1$ component). $M1$–$M6$: thick-filament-based reflections with the 42.9 nm repeat. $Tn1$–$Tn3$: reflections from troponin molecules on the thin filaments. The displacements of the crossbridge projecting levels in the triplets were assumed to be symmetrical. The shape of the function approximated for the crossbridge projection density was also assumed identical in the perturbed and regular regions. The structures of M-line, the titin/connectin molecule and the backbone were neglected. The discrepancy factor (R) for this comparison was ~ 0.1. (R is defined as $\sum_i |I_{obs}(Z_i) - kI_{calc}(Z_i)| / \sum_i |I_{obs}(Z_i)|$, where I_{obs} and I_{calc} denote the observed and calculated intensities, Z_i, the axial coordinate and k [$= \sum_i I_{obs}(Z_i) / \sum_i I_{calc}(Z_i)$] is the scale factor.

taken from our best-fit model. The separation of two projection levels in the triplet was ~ 12.6 nm and the axially projected density width was ~ 11.3 nm. The size of this projected width suggests that the two heads of one myosin crossbridge are tilted away from the plane perpendicular to the fibre axis or that the two heads are tilted asymmetrically away from each other in the opposite (axial) direction as pictured on the left-hand side of Fig. 5(b). The axial width of the C-protein binding region denoted by hatched areas was about 19 nm, suggesting that the C-protein has an axially elongated shape. Fig. 6 shows a comparison of the calculated intensities from our model as compared with the observed one. The present model explains fairly well the positions and intensities of the main thick-filament-based meridional reflections. Note that the structure of the thick-filament backbone was not considered in the present modelling. Although the R factor for this comparison was about 10%, there are some discrepancies between the calculated and observed intensities. These may be improved by introducing other protein components and the backbone structure in the model. Our present model should be compared with that of Malinchik & Lednev (1992).

Figure 5
(a) Arrangement of myosin crossbridge and C-protein molecules on the thick filament (1.6 μm long) in the relaxed frog muscle derived from the analysis of meridional X-ray patterns. In each crossbridge zone there are perturbed regions with an axial period of 42.9 nm (red) in which C-protein binding regions sit (green). Regular regions exist with a separation of 14.3 nm at either distal end (yellow). (b) The axially projected density model of the thick filament in the crossbridge perturbed region is shown on the right-hand side. Each square bar corresponds to the mass density of one crossbridge projecting level projected onto the fibre axis. The axial distance between projection levels in a triplet was ~12.6 nm. The hatched area denotes the C-protein density. On the left-hand side is shown the resting arrangement of two headed myosin crossbridges expected from the model shown on the right (where C-protein molecules are deleted) in which each head structure was modelled from the crystal structure (Rayment et al., 1993).

3. Conclusions

The results reported here serve as a demonstration of the potential benefit of highly collimated X-rays from an

undulator in the Tristan main ring for diffraction from complex systems with long periodicities, such as muscle. The advantage of the high flux was obvious in high time-resolved studies that have been reported elsewhere (Yagi *et al.*, 1996). Together, these studies provide a preview of the expected gains for experiments on small specimens from more widespread use of undulator radiation at third-generation synchrotron sources.

References

Bordas, J., Mant, G. R., Diakun, G. P. & Nave, C. (1987). *J. Cell Biol.* **105**, 1311–1318.

Craig, R., Alamo, L. & Padron, R. (1992). *J. Mol. Biol.* **228**, 474–487.

Haselgrove, J. C. (1975). *J. Mol. Biol.* **92**, 113–143.

Holmes, K. C. (1974). *Endeavour*, **33**, 60–66.

Holmes, K. C. (1989). *Top. Curr. Chem.* **151**, 1–7.

Huxley, H. E. & Brown, W. (1967). *J. Mol. Biol.* **30**, 383–434.

Kamada, S., Fukuma, H., Ogata, A., Isawa, M., Nakamura, N., Sakanaka, S., Tobiyama, M., Kubo, T., Egawa, K., Mitsuhashi, T., Mimashi, T., Kobayashi, M. & Katsura, T. (1995). *Rev. Sci. Instrum.* **66**, 1913–1915.

Malinchik, S. B. & Lednev, V. V. (1992). *J. Muscle Res. Cell Motil.* **13**, 406–419.

Rayment, I., Rypniewski, W. R., Schmidt-Base, K., Smith, R., Tomchick, D. R., Benning, M. M., Winkelmann, D. A., Wesenberg, G. & Holden, H. M. (1993). *Science*, **261**, 50–58.

Rome, E., Offer, G. & Pepe, F. A. (1973). *Nature (London) New Biol.* **244**, 152–154.

Rosenbaum, G., Holmes, K. C. & Witz, J. (1971). *Nature (London)*, **230**, 434–437.

Squire, J. M. (1981). *The Structural Basis of Muscular Contraction*. New York: Plenum.

Stewart, M. & Kensler, R. W. (1986). *J. Mol. Biol.* **192**, 831–851.

Sugiyama, H. (1996). *Proceedings of the Meeting 'The MR Light Source Experiments'*, edited by K. Ohsumi, H. Fukuma & S. Kamada, pp. 88–101. KEK, Tsukuba, Japan. (In Japanese.).

Sugiyama, H., Zhang, X., Higashi, Y., Arakawa, E. & Ando, M. (1998). In preparation.

Tristan Super Light Facility Conceptual Design Report (1992). KEK Progress Report 92–1. KEK, Tsukuba, Japan.

Yagi, N., O'Brien, E. J. & Matsubara, I. (1981). *Biophys. J.* **33**, 121–138.

Yagi, N., Wakabayashi, K., Iwamoto, H., Horiuti, K., Kojima, I., Irving, T. C., Takezawa, Y., Sugimoto, Y., Iwamoto, S., Majima, T., Amemiya, Y. & Ando, M. (1996). *J. Synchrotron Rad.* **3**, 305–312.

Yamamoto, S., Shioya, T., Kitamura, H. & Tsuchiya, K. (1995). *Rev. Sci. Instrum.* **66**, 1996–1998.

Yamamoto, S., Sugiyama, H., Tsuchiya, K. & Shioya, T. (1997). *J. Synchrotron Rad.* **4**, 54–59.

Yamamoto, S., Tsuchiya, K., Shioya, T., Amano, D. & Sugiyama, H. (1998). *J. Synchrotron Rad.* **5**, 462–464.